Nanoscale

PAPER

Cite this: *Nanoscale*, 2023, **15**, 1230

Carrier confinement and interband optical transitions in lead chalcogenide quantum wells, nanosheets, and nanoplatelets

Serguei V. Goupalov [a,b]

Received 28th May 2022,
Accepted 12th December 2022

DOI: 10.1039/d2nr02942a

rsc.li/nanoscale

Analytic equation for energy dispersion of electronic states in lead chalcogenide nanosheets is derived within an effective mass model. Selection rules for interband optical transitions are analyzed and expressions for interband optical matrix elements are obtained. It is shown that the main effect of the lateral confinement in nanoplatelets can be accounted for in terms of the quantized in-plane wave vector.

1. Introduction

Quasi-2D colloidal semiconductor nanosheets and nanoplatelets have recently attracted attention due to their promising optoelectronic properties strongly different from their bulk, quasi-1D, and quasi-0D counterparts.[1] Lead chalcogenide nanosheets and nanoplatelets, along with other lead chalcogenide nanostructures, are of great interest due to their widely size-tunable band gap and photoluminescence from the far-infrared to the near-infrared spectral range. Synthesis and optical spectroscopy of colloidal PbS and PbSe nanosheets and nanoplateletes with rock-salt crystal structure have been reported in a number of studies,[2–6] and their potential for optoelectronics[7–9] and spintronics[10] applications has been demonstrated.

Theoretical investigation of electronic states in lead-salt nanosheets within the $\boldsymbol{k}{\cdot}\boldsymbol{p}$ approximation was performed by Yang and Wise.[11] They started with an isotropic Hamiltonian neglecting band anisotropy and electron–hole Coulomb interaction and then added them as perturbations. In their study they relied on numerical calculations, even for the energy spectrum and eigenstates of the isotropic unperturbed Hamiltonian. However, the main advantage of the $\boldsymbol{k}{\cdot}\boldsymbol{p}$ models is their allowance for fully analytical solutions and possibility to analyze various limiting cases.

In this work we will find the analytical energy dispersion equations for electron and hole states in a PbX (X = S,Se) nanosheet or quantum well (QW), the latter term being mainly used for epitaxially-grown nanostructures. We will consider states in a single L-valley of a lead chalcogenide semiconductor and use the isotropic $\boldsymbol{k}{\cdot}\boldsymbol{p}$ approximation. This approximation is suitable for [001]-grown QWs.[11] We will also discuss interband optical transitions in PbX nanosheets and study how lateral confinement affects electron and hole ground states in PbX nanoplatelets. The electron–hole Coulomb interaction and effect of valley anisotropy can be accounted for using perturbation theory, as shown in ref. 11, and will not be considered here.

[a] Department of Physics, Jackson State University, Jackson, MS 39217, USA. E-mail: serguei.goupalov@jsums.edu

[b] A.F. Ioffe Physico-Technical Institute, 26 Polytechnicheskaya, 194021 St Petersburg, Russia

2. Results and discussion

2.1. Dispersion equation

The conduction and valence band extrema in lead salt semiconductors (PbSe, PbS) occur at the L-points of the Brillouin zone. Electron spectrum near the L-point taking into account only the two closely lying conduction and valence bands and neglecting band anisotropy can be described by the spherical Dimmock model.[11,12] In this model the electron wave function is written as

$$\Psi = \hat{u}|L_6{}^{-}\rangle + \hat{v}|L_6{}^{+}\rangle, \tag{1}$$

where $|L_6{}^{-}\rangle$ and $|L_6{}^{+}\rangle$ describe the Bloch functions while $\hat{u}(\boldsymbol{r})$ and $\hat{v}(\boldsymbol{r})$ are the spinors slowly varying with coordinates and satisfying the equations

$$H\begin{bmatrix}\hat{u}\\ \hat{v}\end{bmatrix} \equiv \begin{bmatrix} \left(\dfrac{E_g}{2} - \alpha_c\Delta\right) & -iP(\boldsymbol{\sigma}\nabla) \\ -iP(\boldsymbol{\sigma}\nabla) & -\left(\dfrac{E_g}{2} - \alpha_v\Delta\right) \end{bmatrix}\begin{bmatrix}\hat{u}\\ \hat{v}\end{bmatrix} = E\begin{bmatrix}\hat{u}\\ \hat{v}\end{bmatrix}. \tag{2}$$

Here σ_β ($\beta = x, y, z$) are the Pauli matrices, α_c, α_v, E_g, and P are parameters of the model and E is the electron energy. We use the atomic system of units, where the electron charge, the electron mass, and the Planck constant $|e| = m_0 = \hbar = 1$. The energy band dispersion in the bulk, resulting from eqn (2), is shown in Fig. 1 assuming, for simplicity, that the only nonzero

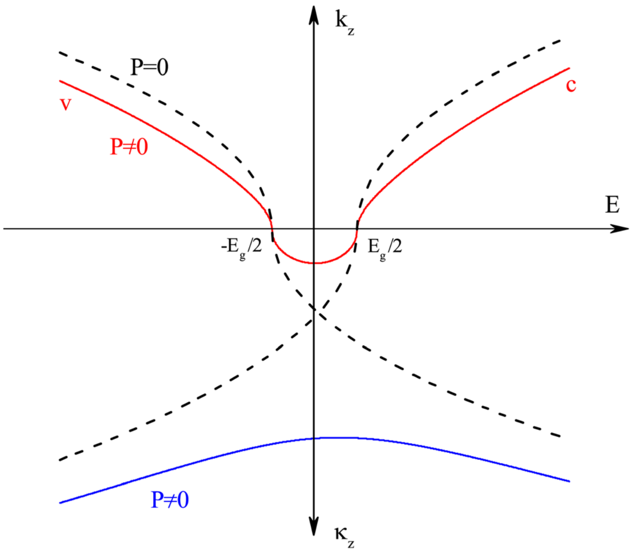

Fig. 1 Scheme of the band energy dispersion in the bulk at zero in-plane wave vector $k = 0$ resulting from eqn (2). To each value of energy E, satisfying $|E| > E_g/2$, there correspond two dispersive branches: one with real k_z (red solid line) and the other with imaginary $k_z = i\kappa_z$ (blue solid line). Dashed black lines correspond to decoupled conduction and valence bands ($P = 0$).

component of the electron quasi-momentum is directed along the z axis.

We will assume that the QW is grown in the z direction, has the width L_z, and represents a PbX slab confined between the planes $z = -L_z/2$ and $z = L_z/2$. Similar to ref. 13, we will construct solutions of eqn (2) in the form of cylindrical waves with the in-plane wave number k and projection of the angular momentum M. We will first consider a solution for which the first component of the bispinor is symmetric with respect to the change $z \to -z$. This implies that the last component of the bispinor is also symmetric while the second and the third components are anti-symmetric.[13] One can construct four independent solutions of eqn (2) satisfying these conditions. We choose the first two of them in the form (*cf.* ref. 13)

$$\hat{u}^{(1)}_{M,k,k_z}(\rho,\varphi,z) = A_1 \cos k_z z \begin{bmatrix} e^{i(M-1/2)\varphi} J_{M-1/2}(k\rho) \\ 0 \end{bmatrix}, \tag{3}$$

$$\hat{v}^{(1)}_{M,k,k_z}(\rho,\varphi,z) = \frac{iPA_1}{\alpha_v k^2 + \alpha_v k_z{}^2 + E + E_g/2} \times \begin{bmatrix} k_z \sin k_z z e^{i(M-1/2)\varphi} J_{M-1/2}(k\rho) \\ k \cos k_z z e^{i(M+1/2)\varphi} J_{M+1/2}(k\rho) \end{bmatrix}, \tag{4}$$

$$\hat{u}^{(2)}_{M,k,k_z}(\rho,\varphi,z) = B_1 \sin k_z z \begin{bmatrix} 0 \\ e^{i(M+1/2)\varphi} J_{M+1/2}(k\rho) \end{bmatrix}, \tag{5}$$

$$\hat{v}^{(2)}_{M,k,k_z}(\rho,\varphi,z) = \frac{iPB_1}{\alpha_v k^2 + \alpha_v k_z{}^2 + E + E_g/2} \times \begin{bmatrix} -k \sin k_z z e^{i(M-1/2)\varphi} J_{M-1/2}(k\rho) \\ k_z \cos k_z z e^{i(M+1/2)\varphi} J_{M+1/2}(k\rho) \end{bmatrix}, \tag{6}$$

where $J_n(x)$ is the Bessel function of order n,

$$k^2 + k_z{}^2 = \Xi + \Lambda, \tag{7}$$
$$\Lambda = \frac{E(\alpha_v - \alpha_c) - P^2 - E_g(\alpha_v + \alpha_c)/2}{2\alpha_c\alpha_v},$$
$$\Xi = \frac{\sqrt{[E(\alpha_v - \alpha_c) - E_g(\alpha_v + \alpha_c)/2 - P^2]^2 + \alpha_c\alpha_v(4E^2 - E_g{}^2)}}{2\alpha_c\alpha_v}.$$

Note that, when $P = 0$, *i.e.* there is no coupling between the conduction and the valence bands,

$$\Xi = \pm \frac{E(\alpha_c + \alpha_v) - E_g(\alpha_v - \alpha_c)/2}{2\alpha_c\alpha_v}. \tag{8}$$

In this limit we obtain $k^2 + k_z{}^2 = \frac{E - E_g/2}{\alpha_c}$, $E = \frac{E_g}{2} + \alpha_c(k^2 + k_z{}^2)$, conduction band state for the upper sign in eqn (8) and $k^2 + k_z{}^2 = \frac{-E - E_g/2}{\alpha_v}$, $E = -\frac{E_g}{2} - \alpha_v(k^2 + k_z{}^2)$, valence band state for the lower sign in eqn (8), *cf.* dashed lines in Fig. 1.

The remaining two solutions are

$$\hat{u}^{(3)}_{M,k,\kappa_z}(\rho,\varphi,z) = C_1 \cosh \kappa_z z \begin{bmatrix} e^{i(M-1/2)\varphi} J_{M-1/2}(k\rho) \\ 0 \end{bmatrix}, \tag{9}$$

$$\hat{v}^{(3)}_{M,k,\kappa_z}(\rho,\varphi,z) = \frac{iPC_1}{\alpha_v k^2 - \alpha_v \kappa_z{}^2 + E + E_g/2} \times \begin{bmatrix} -\kappa_z \sinh \kappa_z z e^{i(M-1/2)\varphi} J_{M-1/2}(k\rho) \\ k \cosh \kappa_z z e^{i(M+1/2)\varphi} J_{M+1/2}(k\rho) \end{bmatrix}, \tag{10}$$

$$\hat{u}^{(4)}_{M,k,\kappa_z}(\rho,\varphi,z) = D_1 \sinh \kappa_z z \begin{bmatrix} 0 \\ e^{i(M+1/2)\varphi} J_{M+1/2}(k\rho) \end{bmatrix}, \tag{11}$$

$$\hat{v}^{(4)}_{M,k,\kappa_z}(\rho,\varphi,z) = \frac{iPD_1}{\alpha_v k^2 - \alpha_v \kappa_z{}^2 + E + E_g/2} \times \begin{bmatrix} -k \sinh \kappa_z z e^{i(M-1/2)\varphi} J_{M-1/2}(k\rho) \\ \kappa_z \cosh \kappa_z z e^{i(M+1/2)\varphi} J_{M+1/2}(k\rho) \end{bmatrix}, \tag{12}$$

where

$$k^2 - \kappa_z{}^2 = \Lambda - \Xi. \tag{13}$$

When $P = 0$, we obtain $k^2 - \kappa_z{}^2 = \frac{-E - E_g/2}{\alpha_v}$, $E = -\frac{E_g}{2} - \alpha_v(k^2 - \kappa_z{}^2)$, conduction band state for the upper sign in eqn (8) and $k^2 - \kappa_z{}^2 = \frac{E - E_g/2}{\alpha_c}$, $E = \frac{E_g}{2} + \alpha_c(k^2 - \kappa_z{}^2)$, valence band state for the lower sign in eqn (8), *cf.* dashed lines in Fig. 1.

Next we impose the boundary condition of the four-component envelope wave function vanishing at $z = L_z/2$. The four solutions we constructed are not mutually orthogonal but they are linearly independent. If one requires that their linear combination (with the coefficients A_1, B_1, C_1, and D_1) vanishes at $z = L_z/2$ then one will obtain a system of four homogeneous algebraic equations on these coefficients. The condition that this system has a non-trivial solution will lead to the dispersion equation determining the allowed energy values of electrons confined in a QW. The positive (negative) values of energy describe the states in the conduction (valence) band. The dispersion equation takes the form

$$\alpha_v^2 k^2 ({k_z}^2 + {\kappa_z}^2)^2 + {k_z}^2 (\alpha_v k^2 - \alpha_v {\kappa_z}^2 + E + E_g/2)^2 - {\kappa_z}^2 (\alpha_v k^2 + \alpha_v {k_z}^2 + E + E_g/2)^2 + k_z \kappa_z (\alpha_v k^2 - \alpha_v {\kappa_z}^2 + E + E_g/2)(\alpha_v k^2 + \alpha_v {k_z}^2 + E + E_g/2) \times \left[\frac{\tanh \frac{\kappa_z L_z}{2}}{\tan \frac{k_z L_z}{2}} - \frac{\tan \frac{k_z L_z}{2}}{\tanh \frac{\kappa_z L_z}{2}} \right] = 0. \tag{14}$$

We note that eqn (14) has the same structure as equations describing the dispersion of elastic Lamb waves in plates[14–18] and of hole states in QWs of III–V or Ge type semiconductors[19] or carrier states in QWs of gapless semiconductors of HgTe type.[19] Although we derived them for cylindrical waves, the same dispersion equations are valid for plane waves.

If we consider solutions of the opposite symmetry with respect to the transformation $z \to -z$, we will obtain the same dispersion equation due to the twofold Kramers degeneracy of the levels.[19]

Let us introduce

$$f(k_z, \kappa_z, k) = \frac{g_1(k_z, \kappa_z, k)}{h_1(k_z, \kappa_z, k)}, \tag{15}$$

$$g_1(k_z, \kappa_z, k) = {\alpha_v}^2 k^2 ({k_z}^2 + {\kappa_z}^2)^2 + {k_z}^2 (\alpha_v k^2 - \alpha_v {\kappa_z}^2 + E + E_g/2)^2 - {\kappa_z}^2 (\alpha_v k^2 + \alpha_v {k_z}^2 + E + E_g/2)^2,$$

$$h_1(k_z, \kappa_z, k) = 2 k_z \kappa_z (\alpha_v k^2 - \alpha_v {\kappa_z}^2 + E + E_g/2) \times (\alpha_v k^2 + \alpha_v {k_z}^2 + E + E_g/2),$$

$$x = \frac{\tan \frac{k_z L_z}{2}}{\tanh \frac{\kappa_z L_z}{2}}.$$

Then eqn (14) takes the form

$$x^2 - 2fx - 1 = 0 \tag{16}$$

or

$$x = f \pm \sqrt{f^2 + 1}. \tag{17}$$

Thus, one can distinguish two different types of solutions. In the limit $k = 0$ these solutions become

$$\frac{\tan \frac{k_z L_z}{2}}{\tanh \frac{\kappa_z L_z}{2}} = \frac{k_z (-\alpha_v {\kappa_z}^2 + E + E_g/2)}{\kappa_z (\alpha_v {k_z}^2 + E + E_g/2)} \tag{18}$$

and

$$\frac{\tan \frac{k_z L_z}{2}}{\tanh \frac{\kappa_z L_z}{2}} = -\frac{\kappa_z (\alpha_v {k_z}^2 + E + E_g/2)}{k_z (-\alpha_v {\kappa_z}^2 + E + E_g/2)}. \tag{19}$$

In the limit of $P = 0$ (and $k = 0$), for the conduction band states, the right-hand side of eqn (18) becomes zero, while the right-hand side of eqn (19) becomes infinite. Thus, for the conduction band states, eqn (18) yields $k_z = 2n\pi/L_z$ and eqn (19) yields $k_z = (2n - 1)\pi/L_z$, where n is a natural number. For the valence-band states, in the same limit the right-hand side of eqn (18) becomes infinite, and the right-hand side of eqn (19) becomes zero. Thus, for the valence band states, eqn (18) yields $k_z = (2n - 1)\pi/L_z$ and eqn (19) yields $k_z = 2n\pi/L_z$. Therefore, eqn (18) gives energies of the odd (*i.e.* 1st, 3rd, *etc.*) levels in the valence band and even (*i.e.* 2nd, 4th, *etc.*) levels in the conduction band while eqn (19) gives energies of the odd levels in the conduction band and even levels in the valence band.

The energy dispersion for the first two subbands in the conduction and valence bands following from eqn (14) are shown in Fig. 2 and 3 for 40 Å thick and 10 Å thick PbS nanosheets, respectively. The material parameters are taken from ref. 11.

The dispersion eqn (14), (18), and (19) explicitly contain only parameter α_v and not α_c. It is not always convenient when analyzing limiting cases. We will see it when we construct the corresponding eigenstates. Therefore, let us obtain an equivalent form of eqn (14) which would contain the parameter α_c. To this end let us consider the following solutions of eqn (2) (*cf.* ref. 13)

$$\hat{u}^{(5)}_{M,k,k_z}(\rho, \varphi, z) = \frac{iPA_2}{\alpha_c k^2 + \alpha_c {k_z}^2 - E + E_g/2} \times \begin{bmatrix} -k_z \sin k_z z e^{i(M-1/2)\varphi} J_{M-1/2}(k\rho) \\ -k \cos k_z z e^{i(M+1/2)\varphi} J_{M+1/2}(k\rho) \end{bmatrix}, \tag{20}$$

$$\hat{v}^{(5)}_{M,k,k_z}(\rho, \varphi, z) = A_2 \cos k_z z \begin{bmatrix} e^{i(M-1/2)\varphi} J_{M-1/2}(k\rho) \\ 0 \end{bmatrix}, \tag{21}$$

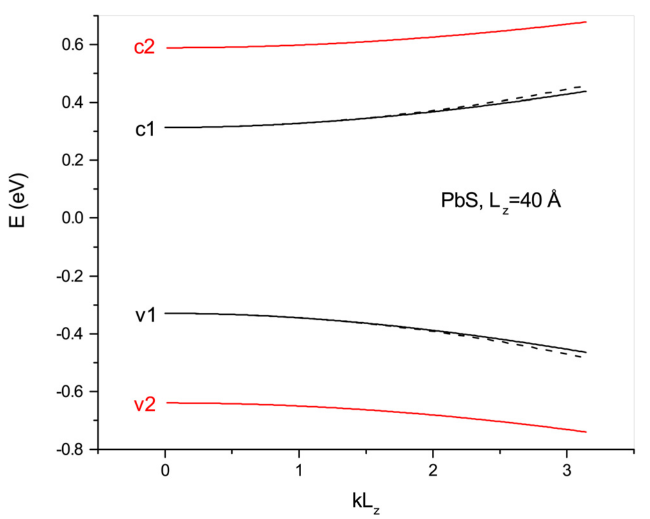

Fig. 2 Energy dispersion curves for first few subbands in a PbS nanosheet of the thickness L_z = 40 Å (solid lines) and their fit with parabolic functions (dashed lines) with the effective masses m_{c1} = 0.163 m_0, m_{c2} = 0.253 m_0, m_{v1} = 0.152 m_0, and m_{v2} = 0.225 m_0. For red curves, solid and dashed lines cannot be resolved at this scale.

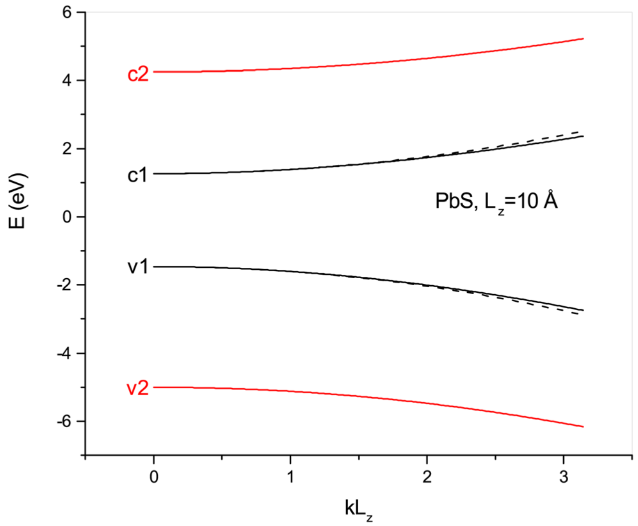

Fig. 3 Same as Fig. 2 but for a PbS nanosheet of the thickness L_z = 10 Å. The effective masses corresponding to the first two conduction-band and valence-band subbands are, respectively, m_{c1} = 0.301 m_0, m_{c2} = 0.385 m_0 and m_{v1} = 0.264 m_0, m_{v2} = 0.322 m_0.

$$\hat{u}^{(6)}_{M,k,k_z}(\rho,\varphi,z) = \frac{iPB_2}{\alpha_c k^2 + \alpha_c {k_z}^2 - E + E_g/2} \times \begin{bmatrix} k \sin k_z z e^{i(M-1/2)\varphi} J_{M-1/2}(k\rho) \\ -k_z \cos k_z z e^{i(M+1/2)\varphi} J_{M+1/2}(k\rho) \end{bmatrix}, \tag{22}$$

$$\hat{v}^{(6)}_{M,k,k_z}(\rho,\varphi,z) = B_2 \sin k_z z \begin{bmatrix} 0 \\ e^{i(M+1/2)\varphi} J_{M+1/2}(k\rho) \end{bmatrix}, \tag{23}$$

$$\hat{u}^{(7)}_{M,k,\kappa_z}(\rho,\varphi,z) = \frac{iPC_2}{\alpha_c k^2 - \alpha_c {\kappa_z}^2 - E + E_g/2} \times \begin{bmatrix} \kappa_z \sinh \kappa_z z e^{i(M-1/2)\varphi} J_{M-1/2}(k\rho) \\ -k \cosh \kappa_z z e^{i(M+1/2)\varphi} J_{M+1/2}(k\rho) \end{bmatrix}, \tag{24}$$

$$\hat{v}^{(7)}_{M,k,\kappa_z}(\rho,\varphi,z) = C_2 \cosh \kappa_z z \begin{bmatrix} e^{i(M-1/2)\varphi} J_{M-1/2}(k\rho) \\ 0 \end{bmatrix}, \tag{25}$$

$$\hat{u}^{(8)}_{M,k,\kappa_z}(\rho,\varphi,z) = \frac{iPD_2}{\alpha_c k^2 - \alpha_c {\kappa_z}^2 - E + E_g/2} \times \begin{bmatrix} k \sinh \kappa_z z e^{i(M-1/2)\varphi} J_{M-1/2}(k\rho) \\ -\kappa_z \cosh \kappa_z z e^{i(M+1/2)\varphi} J_{M+1/2}(k\rho) \end{bmatrix}, \tag{26}$$

$$\hat{v}^{(8)}_{M,k,\kappa_z}(\rho,\varphi,z) = D_2 \sinh \kappa_z z \begin{bmatrix} 0 \\ e^{i(M+1/2)\varphi} J_{M+1/2}(k\rho) \end{bmatrix}. \tag{27}$$

If one requires that a linear combination of these solutions (with the coefficients A_2, B_2, C_2, and D_2) vanishes at $z = L_z = 2$ then one will obtain a system of four homogeneous algebraic equations on these coefficients. The condition that this system has a non-trivial solution will yield an alternative form of the function (15):

$$f(k_z,\kappa_z,k) = \frac{g_2(k_z,\kappa_z,k)}{h_2(k_z,\kappa_z,k)}, \tag{15a}$$

where

$$g_2(k_z,\kappa_z,k) = {\alpha_c}^2 k^2 ({k_z}^2 + {\kappa_z}^2)^2 + {k_z}^2(\alpha_c k^2 - \alpha_c {\kappa_z}^2 - E + E_g/2)^2 - {\kappa_z}^2(\alpha_c k^2 + \alpha_c {k_z}^2 - E + E_g/2)^2,$$

$$h_2(k_z,\kappa_z,k) = 2k_z\kappa_z(\alpha_c k^2 - \alpha_c {\kappa_z}^2 - E + E_g/2) \times (\alpha_c k^2 + \alpha_c {k_z}^2 - E + E_g/2).$$

In the limit of $k = 0$ we obtain

$$\frac{\tan\frac{k_z L_z}{2}}{\tanh\frac{\kappa_z L_z}{2}} = -\frac{\kappa_z(\alpha_c {k_z}^2 - E + E_g/2)}{k_z(-\alpha_c {\kappa_z}^2 - E + E_g/2)}, \tag{18a}$$

$$\frac{\tan\frac{k_z L_z}{2}}{\tanh\frac{\kappa_z L_z}{2}} = \frac{k_z(-\alpha_c {\kappa_z}^2 - E + E_g/2)}{\kappa_z(\alpha_c {k_z}^2 - E + E_g/2)}. \tag{19a}$$

2.2. Interband optical transitions

In order to account for the interband optical transitions we note that usually, for QWs, one can neglect the dependence of the optical matrix element on the in-plane wave number k.[20] Thus, we will continue to consider the limit of k = 0. We will construct the bispinor wave function corresponding to eqn (18) using the solutions (20)–(27). In what follows we will be concerned with the motion along z and neglect normalization factors related to the in-plane motion. Taking into account both components of the Kramers doublet, we obtain

$$\Psi_M(z) = A_2 \begin{bmatrix} \psi(z)\delta_{M,1/2} \\ \psi^*(z)\delta_{M,-1/2} \\ \chi(z)\delta_{M,1/2} \\ \chi(z)\delta_{M,-1/2} \end{bmatrix}, \quad \text{valence band, odd level} \tag{28}$$

where

$$\chi(z) = \cos k_z z - \frac{\cos\frac{k_z L_z}{2}}{\cosh\frac{\kappa_z L_z}{2}} \cosh \kappa_z z, \tag{29}$$

$$\psi(z) = -\frac{iPk_z}{\alpha_c {k_z}^2 - E + E_g/2}\xi(z), \tag{30}$$

$$\xi(z) = \sin k_z z - \frac{\sin\frac{k_z L_z}{2}}{\sinh\frac{\kappa_z L_z}{2}} \sinh \kappa_z z, \tag{31}$$

and A_2 is the real normalization constant. The bispinor wave function corresponding to eqn (19) can be constructed using the solutions (3)–(6), (9)–(12). It is given by

$$\Phi_M(z) = A_1 \begin{bmatrix} \chi(z)\delta_{M,1/2} \\ \chi(z)\delta_{M,-1/2} \\ \varphi(z)\delta_{M,1/2} \\ \varphi^*(z)\delta_{M,-1/2} \end{bmatrix}, \quad \text{conduction band, odd level,} \tag{32}$$

where

$$\varphi(z) = \frac{iPk_z}{\alpha_v {k_z}^2 + E + E_g/2}\xi(z), \tag{33}$$

and A_1 is the real normalization constant. In particular, the ground state in the valence (conduction) band is described by the bispinor (28) [(32)]. In the limit $P = 0$ it corresponds to $k_z = \pi/L_z$. Then $\chi(z) = \cos \pi z/L_z$, $\psi(z) = 0$, $\varphi(z) = 0$. We emphasize that, for the ground states, $\psi(z)$ and $\varphi(z)$ appear as a result of the band coupling and are linear in P. For even levels (*i.e.* 2nd, 4th, *etc.*) in the conduction or valence bands, denominators in expressions (30), (33) diverge at $P = 0$ and another form of the wave functions is more revealing. In particular, we obtain another bispinor wave function corresponding to eqn (18)

$$\tilde{\Psi}_{\mathrm{M}}(z) = B_1 \begin{bmatrix} \xi(z)\delta_{\mathrm{M},1/2} \\ \xi(z)\delta_{\mathrm{M},-1/2} \\ \tilde{\psi}(z)\delta_{\mathrm{M},1/2} \\ \tilde{\psi}^*(z)\delta_{\mathrm{M},-1/2} \end{bmatrix}, \quad \text{conduction band, even level} \tag{34}$$

where

$$\tilde{\psi}(z) = -\frac{iPk_z}{\alpha_v k_z^2 + E + E_g/2}\chi(z) \tag{35}$$

and B_1 is the real normalization constant. For example, in the limit of $P = 0$, the first excited state in the conduction band corresponds to $k_z = 2\pi/L_z$. Then $\xi(z) = \sin 2\pi z/L_z$, $\tilde{\psi}(z) = 0$. When $P \neq 0$ then either of the solutions (28), (34) can be used. Finally, another bispinor wave function corresponding to eqn (19) is

$$\tilde{\Phi}_{\mathrm{M}}(z) = B_2 \begin{bmatrix} \tilde{\varphi}(z)\delta_{\mathrm{M},1/2} \\ \tilde{\varphi}^*(z)\delta_{\mathrm{M},-1/2} \\ \xi(z)\delta_{\mathrm{M},1/2} \\ \xi(z)\delta_{\mathrm{M},-1/2} \end{bmatrix}, \quad \text{valence band, even level,} \tag{36}$$

where

$$\tilde{\varphi}(z) = \frac{iPk_z}{\alpha_c k_z^2 - E + E_g/2}\chi(z), \tag{37}$$

and B_2 is the real normalization constant. If $P \to 0$ then $A_1, B_1, A_2, B_2 \to \sqrt{2/L_z}$.

Due to the parity of the functions $\chi(z)$, $\xi(z)$, the optical transitions occur between odd or between even levels in the valence and conduction bands (*i.e.* 1st to 1st, 1st to 3rd, 2nd to 2nd, *etc.*).

The velocity operator is given by[21]

$$\boldsymbol{v} = \begin{bmatrix} -2i\alpha_c\nabla & P\boldsymbol{\sigma} \\ P\boldsymbol{\sigma} & 2i\alpha_v\nabla \end{bmatrix}. \tag{38}$$

For the matrix element between the bispinor functions (32) and (28) we obtain

$$\begin{aligned} \langle \Phi_{1,M_1}|\boldsymbol{v}|\Psi_{2,M_2}\rangle = A_1A_2 \int_{-L_z/2}^{L_z/2} \mathrm{d}z \big[\delta_{\mathrm{M}_1,\mathrm{M}_2} \Big(P\chi_1\chi_2 \\ -2i\alpha_c\chi_1 \frac{\partial\psi_2}{\partial z} + 2i\alpha_v\varphi_1^* \frac{\partial\chi_2}{\partial z} + P\varphi_1^*\psi_2 \Big) \boldsymbol{e}_z(\delta_{\mathrm{M}_1,1/2} - \delta_{\mathrm{M}_1,-1/2}) \\ +\delta_{\mathrm{M}_1,-\mathrm{M}_2} P(\chi_1\chi_2 + \varphi_1\psi_2)(\delta_{\mathrm{M}_1,1/2}(\boldsymbol{e}_x - i\boldsymbol{e}_y) + \delta_{\mathrm{M}_1,-1/2}(\boldsymbol{e}_x + i\boldsymbol{e}_y)) \big], \end{aligned} \tag{39}$$

where $\boldsymbol{e}_\beta$ is the Cartesian unit vector ($\beta = x, y, z$). For the in-plane light polarization, the main contribution to the optical matrix element, which is linear in P, stems from the term $P\chi_1\chi_2$. However, when light is polarized along the growth direction, there are two additional terms of the same order in P and proportional to α_c and α_v, respectively. Let us analyze the limit of small P and consider the transition between ground states in the valence and conduction bands in the lowest order in P. We obtain

$$\langle \Phi_{1/2}|v_z|\Psi_{1/2}\rangle = P\frac{E_g - (\alpha_c + \alpha_v)\pi^2/L_z^2}{E_g + (\alpha_c + \alpha_v)\pi^2/L_z^2} \tag{40}$$

while taking into account only the term $P\chi_1\chi_2$ would yield $\langle \Phi_{1/2}|v_z|\Psi_{1/2}\rangle = P$. For the matrix element of the z-component of the coordinate operator one has

$$\begin{aligned} \langle \Phi_{1,\mathrm{M}_1}|z|\Psi_{2,\mathrm{M}_2}\rangle =& A_1A_2\delta_{\mathrm{M}_1,\mathrm{M}_2}(\delta_{\mathrm{M}_1,1/2} - \delta_{\mathrm{M}_1,-1/2}) \\ &\times \int_{-L_z/2}^{L_z/2} dz(\chi_1 z\psi_2 + \varphi_1^* z\chi_2). \end{aligned}$$

In the same limit of small P and transition between the ground states one has

$$\langle \Phi_{1/2}|z|\Psi_{1/2}\rangle = -iP\frac{E_g - (\alpha_c + \alpha_v)\pi^2/L_z^2}{(E_g + (\alpha_c + \alpha_v)\pi^2/L_z^2)^2} \tag{41}$$

in agreement with the general quantum-mechanical relation

$$v_z = i(Hz - zH).$$

When $P \to 0$, the conduction and valence bands are decoupled. For small P, the interband dipole matrix element is proportional to P, but band coupling is also proportional to P. As a result, the matrix element (40) is different from P. The terms proportional to α_c and α_v also appear in the expression for the interband velocity matrix element for PbX quantum dots.[21] Similar to the present case, they reduce the interband velocity matrix element and decrease by absolute value with increase of the quantum dot size (*cf.* Fig. 1 in ref. 21).

The matrix element between the bispinor functions (34) and (36), $\langle \tilde{\Psi}_{1,\mathrm{M}_1}|\boldsymbol{v}|\tilde{\Phi}_{2,\mathrm{M}_2}\rangle$ can be obtained from eqn (39) by changing $\chi(z) \to \xi(z)$, $\phi(z) \to \tilde{\psi}(z)$, $\psi(z) \to \tilde{\phi}(z)$, $A_1 \to B_1$, $A_2 \to B_2$.

2.3. Lateral confinement

Finally, let us analyze the effect of the lateral confinement on the energies of the electron and hole ground states. To this end, instead of a quasi-2D nanosheet, we will consider a nanoplatelet in a form of a disc with the radius R and thickness L_z and use the numerical procedure described in details in ref. 22. In case of a quantum box of the size L with the confinement in one spacial dimension, one gets quantization of the wave vector with the quantum of π/L. In case of a disc, such characteristic length can be estimated from the condition $L^2 = \pi R^2$ which yields the quantum of the wave number of $\sqrt{\pi}/R$. In Fig. 4 we change the disc radius from $R = 200\ L_z$ down to $R = L_z$ and plot the electron and hole ground state energies in a PbS disc of the thick-

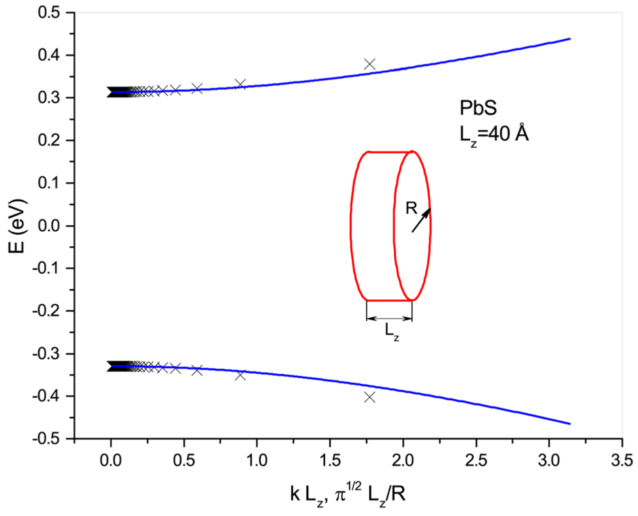

Fig. 4 Electron and hole ground state energies in a PbS disc of changing radius R (from R = 200 L_z down to R = L_z) and fixed thickness L_z = 40 Å (symbols) as functions of the parameter $\sqrt{\pi}/R{\cdot}L_z$ along with energy dispersion curves (lines) for the lowest conduction-band and the uppermost valence-band subbands of a PbS nanosheet of the same thickness as functions of kL_z.

ness L_z = 40 Å as functions of the parameter $\sqrt{\pi}/R{\cdot}L_z$. This allows us to compare these energies with the energy dispersion of the lowest conduction and uppermost valence subbands in a quasi-2D nanosheet of the same thickness plotted in Fig. 4 as functions of the dimensionless wave number kL_z. One can see that the effect of lateral confinement beyond quantization of the in-plane wave number is only important when the lateral size becomes comparable with the disc thickness. Meanwhile, this comparison provides an independent verification of our analytical results.

3. Conclusions

To conclude, we have considered the $\boldsymbol{k}{\cdot}\boldsymbol{p}$ model describing band structure of lead chalcogenide semiconductors and accounting for the coupling between the conduction and valence bands. Within this model, we have found analytic equations for the electron and hole energy dispersion in subbands resulting from the carrier confinement in a PbX nanosheet or QW. Our treatment yields analytical expressions for the bispinor envelope wave functions describing quantum confinement along the quantization direction and provides in-plane effective masses for the electrons and holes in the subbands. These are key ingredients for constructing a robust analytical theory of excitons in these materials[11,20] which would enable fully analytical solutions of many problems relevant to optical spectroscopy, *e.g.* resonant light reflection and transmission.[20,23] We obtained selection rules for interband optical transitions and showed that the main effect of the lateral confinement in nanoplatelets can be accounted for in terms of the quantized in-plane wave vector.

Conflicts of interest

There are no conflicts to declare.

Acknowledgements

The author wishes to thank M.O. Nestoklon for useful discussions. This work was supported by NSF through DMR- 2100248.

References

1 M. Nasilowski, B. Mahler, E. Lhuillier, S. Ithurria and B. Dubertret, *Chem. Rev.*, 2016, **116**, 10934–10982.
2 H. Zhang, B. H. Savitzky, J. Yang, J. T. Newman, K. A. Perez, B.-R. Hyun, L. F. Kourkoutis, T. Hanrath and F. W. Wise, *Chem. Mater.*, 2016, **28**, 127–134.
3 A. H. Khan, R. Brescia, A. Polovitsyn, I. Angeloni, B. Martín-García and I. Moreels, *Chem. Mater.*, 2017, **29**, 2883–2889.
4 J. Lauth, M. Failla, E. Klein, C. Klinke, S. Kingeg and L. D. A. Siebbeles, *Nanoscale*, 2019, **11**, 21569–21576.
5 F. M. Vázquez, Q. Yu, L. F. Klepzig, L. D. A. Siebbeles, R. W. Crisp and J. Lauth, *J. Phys. Chem. Lett.*, 2021, **12**, 680–685.
6 L. F. Klepzig, L. Biesterfeld, M. Romain, A. Niebur, A. Schlosser, J. Hübner and J. Lauth, *Nanoscale Adv.*, 2022, **4**, 590–599.
7 S. Dogan, T. Bielewicz, Y. Cai and C. Klinke, *Appl. Phys. Lett.*, 2012, **101**, 073102.
8 T. Bielewicz, S. Dogan and C. Klinke, *Small*, 2015, **11**, 826–833.
9 S. Dogan, T. Bielewicz, V. Lebedeva and C. Klinke, *Nanoscale*, 2015, **7**, 4875–4883.
10 M. M. Ramin Moayed, T. Bielewicz, M. S. Zöllner, C. Herrmann and C. Klinke, *Nat. Commun.*, 2017, **8**, 15721.
11 J. Yang and F. W. Wise, *J. Phys. Chem. C*, 2015, **119**, 26809–26816.
12 I. Kang and F. W. Wise, *J. Opt. Soc. Am. B*, 1997, **14**, 1632–1646.
13 S. V. Goupalov, *Phys. Rev. B: Condens. Matter Mater. Phys.*, 2011, **84**, 037303.
14 J. W. S. Rayleigh, *Proc. Lond. Math. Soc.*, 1888, **s1–20**, 225–237.
15 H. Lamb, *Proc. Lond. Math. Soc.*, 1889, **s1–21**, 70–90.
16 H. Lamb, *Proc. R. Soc. London, Ser. A*, 1917, **93**, 114–128.
17 S. V. Goupalov, *Phys. Usp.*, 2020, **63**, 57–65.
18 S. V. Goupalov, *J. Phys. Chem. C*, 2019, **123**, 11926–11932.
19 M. I. D'yakonov and A. V. Khaetskii, *Sov. Phys. JETP*, 1982, **55**, 917–920.
20 E. L. Ivchenko, *Optical Spectroscopy of Semiconductor Nanostructures*, Alpha Science, Harrow, U.K., 2005.
21 S. V. Goupalov, E. L. Ivchenko and M. O. Nestoklon, *Phys. Rev. B*, 2022, **106**, 125301.
22 S. V. Goupalov, *J. Phys. Chem. C*, 2013, **117**, 6476–6479.
23 L. C. Andreani, F. Tassone and F. Bassani, *Solid State Commun.*, 1991, **77**, 641–645.